ChemElectroChem

Research Article
doi.org/10.1002/celc.202300662

Chemistry Europe
European Chemical Societies Publishing

www.chemelectrochem.org

Effects of Solvent and Monomer on the Kinetics of Radical Generation in Atom Transfer Radical Polymerization

Marco Fantin,[a] Enrico Tognella,[a] Andrea Antonello,[a] Francesca Lorandi,[a] Elia Calore,[a] Angelika Macior,[a, b] Christian Durante,[a] and Abdirisak A. Isse*[a]

Dedicated to Prof. Flavio Maran on the occasion of his retirement and in recognition of his contribution to molecular electrochemistry

Unlike classical radical polymerization, the kinetics of atom transfer radical polymerization show significant solvent dependence, possibly arising from solvent effects on the activation step. A kinetic study on the activation of the initiator ethyl α-bromoisobutyrate by $[Cu^{I}TPMA]^{+}$ (TPMA = tris(2-pyridylmethyl)amine), an initiator/catalyst combination frequently used in ATRP, was carried out in DMSO, DMF, MeCN, anisole, ethyl acetate, and their 50 vol% mixtures with styrene (STY) and methyl methacrylate (MMA). k_{act} values varying about 3 orders of magnitude from 3.14×10^{5} $mol^{-1}\,dm^{3}\,s^{-1}$ in DMSO to 9.41×10^{2} $mol^{-1}\,dm^{3}\,s^{-1}$ in ethyl acetate were found. These values showed excellent correlation with the solvent polarity/polarizability parameter π*. The effect of MMA or STY depended on polarity compatibility between the monomer and the solvent: After monomer addition, k_{act} decreased considerably in polar solvents, whereas it was almost unaffected in nonpolar solvents.

Introduction

Atom transfer radical polymerization (ATRP) is one of the most important methods of controlled radical polymerization for the synthesis of well-defined polymeric materials with tailored properties for various specific applications.[1,2] Control over chain growth and molecular weight distribution is gained during polymerization due to an equilibrium between a dormant species P_n-X (usually X = Cl or Br) and a propagating radical $P_n^{\bullet}$, mediated by a transition metal complex such as Cu with a polydentate amine ligand (Scheme 1). The equilibrium is well shifted to the left ($K_{ATRP} = k_{act}/k_{deact} \ll 1$), which makes the concentration of the propagating radicals so low that radical-radical termination reactions are very slow. The process begins with a reaction between an alkyl halide initiator (RX) and the metal complex at a low oxidation state, e.g., $[Cu^{I}L]^{+}$. This initiation reaction produces an alkyl radical, which adds to monomer molecules generating a radical polymer chain, $P_n^{\bullet}$, and the metal complex at a higher oxidation state, with the halogen atom bound to the metal center, $[XCu^{II}L]^{+}$. After a short time of reaction, $P_n^{\bullet}$ is deactivated by $[XCu^{II}L]^{+}$ to produce a dormant polymer chain, P_n-X, and the metal at the lower oxidation state. Polymerization proceeds intermittently through short periods between activation and deactivation. The mechanism of the activation step has been widely investigated showing that it occurs by a halogen atom transfer or formally inner-sphere electron transfer.[3–6]

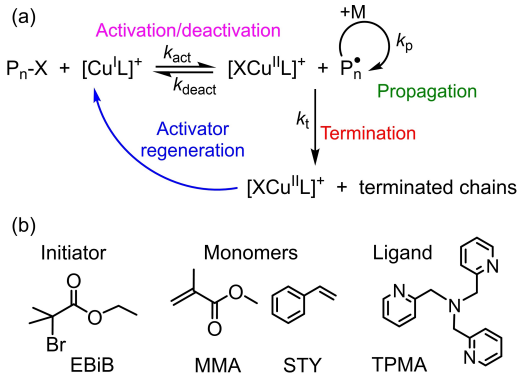

Scheme 1. ATRP mechanism and chemical structures of monomers, initiator, and ligand considered in this work.

Since its inception about three decades ago,[7,8] interest for this polymerization method has been steadily growing and today many variants of ATRP with ppm amounts of metal catalyst are widely used.[9] Many transition metal-based catalysts, such as complexes of Co, Cu, Fe, Ni, Os, Re and Ru, have been tested and found to exhibit good catalytic performance.[10] However, the most widely used catalysts are copper complexes with polydentate nitrogen-based ligands because of ease of preparation (often by in situ mixing of a Cu(II) salt with a ligand)

[a] Dr. M. Fantin, E. Tognella, A. Antonello, Dr. F. Lorandi, E. Calore, A. Macior, Prof. C. Durante, Prof. A. A. Isse
Department of Chemical Sciences, University of Padova
Via Marzolo 1, 35131 Padova, Italy
E-mail: abdirisak.ahmedisse@unipd.it

[b] A. Macior
Department of Physical Chemistry, Rzeszow University of Technology
Al. Powstancow Warszawy 6, 35-959 Rzeszow, Poland

Supporting information for this article is available on the WWW under https://doi.org/10.1002/celc.202300662

and high activity, which is tunable through modification of ligand structure.[11] Recently, iron-based catalysts, albeit being much less active than copper-amine complexes, have attracted considerable attention because Fe is a cheap and abundant metal that can be used even without any added organic ligand.[12–17] Photo-induced ATRP using copper catalysts[18–20] or without any metal catalyst is also widely used.[21–23]

The activation step, in which the propagating radical is generated, plays a crucial role in the rate of polymerization. Similarly, the deactivation step is essential because it avoids uncontrolled radical propagation, as seen in free radical polymerization. However, this step hardly represents a critical issue for Cu-catalyzed ATRP in organic solvents because $[X Cu^{II} L]^+$ is a very efficient radical scavenger with deactivation rate constants of the order of 10^5–10^7 $mol^{-1} dm^3 s^{-1}$.[24] k_{deact} is very high also in aqueous solutions,[25] but in such media the deactivation step might not be efficient because of instability of $[X Cu^{II} L]^+$.[26] ATRP activation kinetics have been intensively investigated in acetonitrile, showing that k_{act} is affected by various factors including alkyl halide initiator structure (RX), type of halogen atom in RX, and amine ligand structure.[27–32] Activation rate constants for several initiator/Cu(I) systems have also been reported in aqueous media.[25,33,34] Comparing k_{act} values in acetonitrile and water showed that activation rate constants are 2–3 orders of magnitude higher in water than in acetonitrile. In good accordance with these findings, we have recently shown that addition of 10 vol% water to acetonitrile induces a 4-fold enhancement of k_{act}.[35]

Although ATRP is performed in many organic solvents, studies on activation kinetics in solvents other than acetonitrile are limited. Some data have been reported in DMF[35–37] and DMSO[35,36,38] and a rapid screening of these data, together with k_{act} values in acetonitrile and water, shows that ATRP kinetics is strongly affected by the reaction medium. Horn and Matyjaszewski[39] examined ATRP activation kinetics in an extended series of solvents showing that the rate constant diminishes with decreasing solvent polarity. Although this work provided valuable information for a deeper understanding of ATRP kinetics, the measured rate constants could better be described as observed values, k_{obs}, rather than true k_{act}. Indeed, while measuring k_{act} requires investigating the kinetics of $[Cu^I L]^+$ with RX, all experiments were performed in solutions containing $Cu^I Br$, ligand and RX. It has been previously reported that halide ions form complexes with Cu ions both in the absence and presence of amine ligands.[40] Therefore, mixing $Cu^I Br$ with the ligand produces different Cu(I) species, mainly $[Cu^I L]^+$ and $[BrCu^I L]$, of which only $[Cu^I L]^+$ is involved in the activation step.[41] Kinetic analysis in the presence of halide ions are conditioned by the presence of speciation equilibria and may not provide true k_{act} values. Indeed, it has been previously reported that the observed rate constants, k_{obs}, for several CuX/L + RX systems depended on $[X^-]$. Consequently, k_{obs} were lower than the true k_{act} values measured with $[Cu^I L]^+$ as the only Cu(I) species present in solution.[41] It must be stressed however that, in some control experiments, Horn and Matyjaszewski found similar k_{act} values in the absence and presence of bromide ions. Another important consideration for further studies on solvent effect on k_{act} is the choice of the Cu complex. The previous study used L = 1,1,4,7,10,10-hexamethyltriethylenetetramine, which gives one of the least active ATRP Cu catalysts that is rarely used. Indeed, the measured rate constants were low (4.14×10^{-2} $mol^{-1} dm^3 s^{-1}$ – 1.3 $mol^{-1} dm^3 s^{-1}$). More active catalysts based on tris[2-(dimethylamino)ethyl]amine (Me_6TREN) and tris(2-pyridylmethyl)amine (TPMA) are widely used today and are more appropriate for studies of solvent effects on activation kinetics. Recently, linear regression techniques have been employed to build comprehensive models for the prediction of k_{act} values.[42] These models were built on a library of k_{act} data comprising structurally diverse initiators and catalysts, whereas the solvent scope was rather narrow and limited to polar media. Moreover, mixtures of solvent and monomer were not considered. Larger datasets spanning a broader range of solvents and solvent/monomer mixtures would enable these data-driven regression methods to more accurately capture the medium effect in ATRP. Therefore, here we chose TPMA as ligand and determined k_{act} for the activation of ethyl α-bromoisobutyrate (EBiB) by $[Cu^I L]^+$ in 5 selected solvents and their 50 vol% mixtures with methyl methacrylate and styrene (Scheme 1b).

Results and Discussion

Redox Behavior of Copper Complexes

Before discussing the redox behavior of copper complexes, it is important to note that Cu(II) is usually pentacoordinated, whereas the preferred coordination number of Cu(I) is 4.[43] Since TPMA is a tetradentate ligand, a solvent molecule will act as the fifth ligand ($[Cu^{II}TPMA(solvent)]^{2+}$) when bromide ions are not present in solution. Although the involvement of solvent molecules in Cu(II) complexes with amine ligands used as ATRP catalysts is well-known,[44] the complexes are often written simply as $[Cu^{II} L]^{2+}$. Accordingly, we will indicate the Cu(II)/TPMA solvato complex simply as $[Cu^{II}TPMA]^{2+}$. In all investigated media both $[Cu^{II}TPMA]^{2+}$ and $[BrCu^{II}TPMA]^+$ exhibited a reversible peak couple assigned to one-electron reduction of Cu(II) to Cu(I). Examples of typical responses in cyclic voltammetry (CV) are reported in Figure 1. In general, both complexes undergo a quasi-reversible electron transfer and the standard potential, calculated from cyclic voltammetry as $E_{1/2} = (E_{pc} + E_{pa})/2$ or from linear sweep voltammetry at a rotating disk electrode, falls in the range from −0.38 V to −0.62 V vs Fc^+/Fc for $[Cu^{II}TPMA]^{2+}$ and −0.66 V to −0.78 V vs Fc^+/Fc for $[BrCu^{II}TPMA]^+$ (Tables S1 and S2). For the $[Cu^{II}TPMA]^{2+}/[Cu^{I}TPMA]^+$ couple, $E_{1/2}$ in MeCN is 0.2 V less negative than in DMF and DMSO. The presence of MMA or STY anodically shifts $E_{1/2}$ up to 0.11 V, depending on monomer and solvent. $E_{1/2}$ of $[BrCu^{II}TPMA]^+/[BrCu^{I}TPMA]$ is always more negative than that of $[Cu^{II}TPMA]^{2+}/[Cu^{I}TPMA]^+$ on account of the higher affinity of Br^- for Cu(II) than Cu(I).[40] The presence of monomers shifts $E_{1/2}$ of $[BrCu^{II}TPMA]^+/[BrCu^{I}TPMA]$ to slightly more negative values (4–43 mV) possibly because of variations of binding constants of $[Cu^{II}TPMA]^{2+}$ and $[Cu^{I}TPMA]^+$ with Br^-

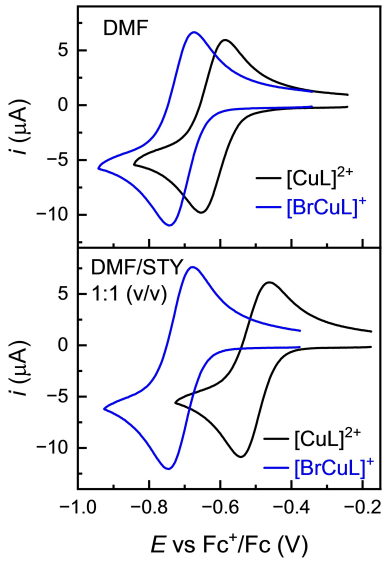

Figure 1. Cyclic voltammetry of 10^{-3} M $[Cu^{II}TPMA]^{2+}$ and $[BrCu^{II}TPMA]^{+}$ in DMF or DMF/STY (1:1, v/v) + 0.1 M Et_4NBF_4, recorded on a GC electrode at $v = 0.1$ V/s.

(*vide infra*). In nonpolar solvents, the presence of monomers has little effect on $E_{1/2}$ of $[BrCu^{II}TPMA]^{+}$ reduction. Further analysis of medium effects on $E_{1/2}$ was not pursued as it is related to multiple parameters including solvent coordination to the copper center, relative halidophilicities of Cu(II) and Cu(I) and non-specific solvation effects.

As we shall see later, the standard electron transfer rate constant, k°, is required for the determination of k_{act} in DMSO, DMF, MeCN and their mixtures with the monomers. Data for most of these systems were previously reported,[45] whereas k° for the remaining systems were determined according to the method of Nicholson (Figure S1).[46] Overall, k° values in the range 7.6×10^{-3} cm s^{-1}–7.5×10^{-2} cm s^{-1} for $[Cu^{II}TPMA]^{2+}$ and 2.3×10^{-2} cm s^{-1}–1.15×10^{-1} cm s^{-1} for $[BrCu^{II}TPMA]^{+}$ were found (Table S1).

Determination of k_{act} by Rotating Disk Electrode

The kinetics of relatively slow reactions were studied by monitoring the concentration of $[Cu^{I}TPMA]^{+}$ by a rotating disk electrode (RDE). The reactions were performed in the presence of a large excess of 2,2,6,6-tetramethyl-1-piperidinyloxy (TEMPO) as a radical trap. The mechanism of the reaction between an initiator RX and $[Cu^{I}L]^{+}$ in the presence of TEMPO is illustrated in Scheme 2. The radical R$^{\bullet}$ generated in the activation step decays through three competing pathways: deactivation back to RX (k_{deact}), coupling with the radical scavenger (k_c), and radical-radical coupling (or disproportionation) yielding termination products (k_t). Before deactivation via one of these pathways, the radical may propagate for a short time if a monomer is present in the reaction medium. The rate constant of deactivation, k_{deact}, by $[XCu^{II}TPMA]^{+}$ is of the order of 10^{6}–10^{8} mol^{-1} dm^{3} s^{-1},[31,36] whereas the rate constant of

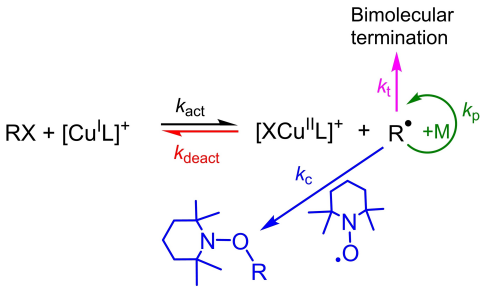

Scheme 2. Mechanism of RX activation in the presence of TEMPO

trapping by TEMPO is near the diffusion-controlled limit.[47,48] Bimolecular radical termination has also a very high rate constant ($k_t = 10^{8}$–10^{9} mol^{-1} dm^{3} s^{-1}).[49] Nevertheless, this deactivation pathway cannot compete with the others because its rate is proportional to $C^{2}_{R^{\bullet}}$, which is very low. As to the other two R$^{\bullet}$ decay routes, $k_c > k_{deact}$ and, if excess TEMPO is used, $C_{TEMPO} >> C_{[XCu^{II}L]^{+}}$, the rate of radical capture by TEMPO will be much higher than the deactivation rate by $[XCu^{II}L]^{+}$. The propagation reaction can occur only in solvent/monomer mixtures, but its rate is negligible in the presence of the radical scavenger. Therefore, the overall process can be considered as a two-step reaction in which the activation step is followed by a very fast and irreversible R$^{\bullet}$ capture by TEMPO. The activation step is the rate-determining step, and the rate law becomes (see Supporting Information):

$$v = -dC_{[Cu^{I}L]^{+}}/dt = k_{act}C_{[Cu^{I}L]^{+}}C_{RX} \quad (1)$$

which is integrated to give

$$1/C - 1/C_0 = k_{act}t \quad (2)$$

if $[Cu^{I}L]^{+}$ and RX have the same initial concentration, C_0.

The details of the experimental setup have previously been reported.[31,41] Equimolar amounts of $[Cu^{I}TPMA]^{+}$ and ethyl α-bromoisobutyrate (EBiB) were mixed in the chosen reaction medium in the presence of a 20-fold excess of TEMPO and the anodic limiting current for the oxidation of $[Cu^{I}TPMA]^{+}$ to $[Cu^{II}TPMA]^{2+}$ was recorded on a glassy carbon rotating disk electrode to monitor the decay of Cu(I) concentration. The initial concentration of $[Cu^{I}TPMA]^{+}$ and EBiB was 10^{-4} mol dm^{-3} and the applied potential was $E_{1/2} + 0.3$ V so that the oxidation process was under diffusion control and the Levich equation could be used to calculate Cu(I) bulk concentration, C, from the limiting current, i_L:

$$i_L = 0.62nFAD^{1/2}\omega^{2/3}\nu^{-1/6}C \quad (3)$$

where D is the diffusion coefficient of $[Cu^{I}TPMA]^{+}$, ω is the angular velocity of the rotating electrode and ν is the kinematic viscosity of the medium.

Examples of limiting current decay during activation of EBiB by $[Cu^{I}TPMA]^{+}$ are reported in Figure 2a. After converting i_L to C, the reaction kinetics were analyzed according to a second-

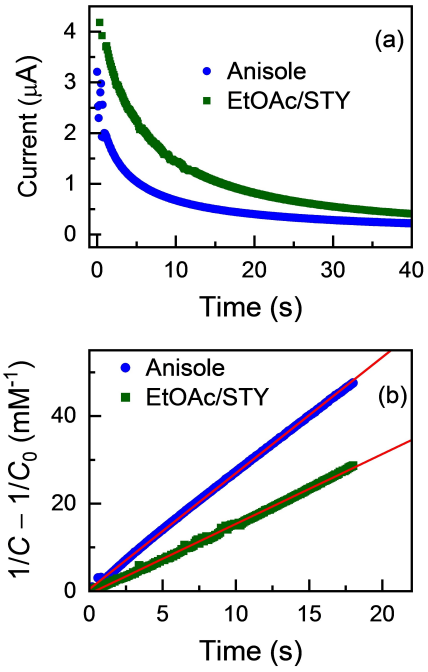

Figure 2. (a) Chronoamperometry of 10^{-4} M $[Cu^{I}TPMA]^{+}$ + 10^{-4} M EBiB + 2×10^{-3} M TEMPO in anisole or EtOAc/styrene (1:1, v/v) in the presence of 0.2 M *n*-Bu_4NBF_4, recorded on a GC rotating disc electrode at $\omega = 4000$ rpm. (b) Kinetic analysis according to a second-order rate law.

order rate law. Plots of $(1/C - 1/C_0)$ vs time gave straight lines with slopes corresponding to k_{act} values. Two examples of this analysis are shown in Figure 2b, whereas plots for all systems investigated with this technique are reported in Figure S2. This method is appropriate for the determination of low to moderately high k_{act} values. It was applied to reactions in anisole, ethyl acetate (EtOAc), and various solvent/monomer mixtures, and the results are reported in Table 1.

Table 1. Rate constants for the reaction between $[Cu^{I}TPMA]^{+}$ and ethyl α-bromoisobutyrate at 25 °C.

Entry	Solvent	Monomer[a]	Method[b]	logk_{act} [c]
1	EtOAc	–	RDE	2.97
2	EtOAc	MMA	RDE	3.00
3	EtOAc	STY	RDE	3.13
4	Anisole	–	RDE	3.42
5	Anisole	MMA	RDE	3.30
6	Anisole	STY	RDE	3.31
7	MeCN	–	HRC	4.02
8	MeCN	STY	RDE	3.18
9	MeCN	STY	HRC	2.98
10	MeCN	MMA	RDE	3.20
11	MeCN	MMA	HRC	3.00
12	DMF	–	HRC	4.79
13	DMF	STY	RDE	3.13
14	DMF	STY	HRC	3.36
15	DMF	MMA	HRC	3.15
16	DMSO	–	HRC	5.50
17	DMSO	STY	HRC	4.61
18	DMSO	MMA	HRC	3.79

[a] MMA = methyl methacrylate; STY = styrene, both at 50 vol%. [b] RDE: chronoamperometry for Cu(I) oxidation on a rotating disk electrode; HRC: voltammetric analysis of homogeneous redox catalysis. [c] k_{act} in $mol^{-1}\,dm^3\,s^{-1}$.

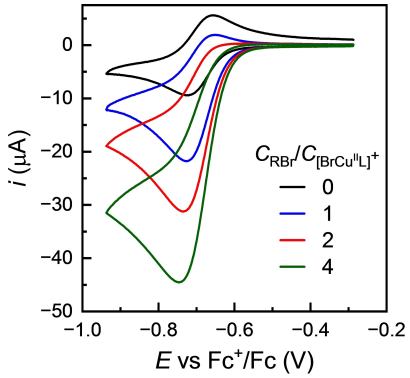

Figure 3. Cyclic voltammetry of 10^{-3} M $[Br Cu^{II}TPMA]^{+}$ in DMSO + 0.1 M Et_4NBF_4, recorded on a GC electrode at $v = 0.1$ V/s in the absence and presence of ethyl α-bromoisobutyrate (RBr) at different concentrations together with 2×10^{-2} M TEMPO.

Determination of k_{act} by Cyclic Voltammetry

Reactions of $[Cu^{I}TPMA]^{+}$ with EBiB in MeCN, DMF, DMSO and some of their mixtures with monomers were too fast to be investigated by the RDE technique. The activation kinetics in these media were investigated by cyclic voltammetry using as catalyst $[Br Cu^{II}TPMA]^{+}$ prepared in situ by mixing equimolar amounts of Cu(II) triflate, TPMA and Et_4NBr as a source of bromide ions. This system presents a reversible peak couple, which is not affected by addition of a large excess of TEMPO. Instead, addition of EBiB to the solution causes drastic changes to the voltammetric pattern of $[Br Cu^{II}TPMA]^{+}$. The cathodic peak increases in height while the intensity of its anodic partner decreases until it disappears in the presence of excess initiator, indicating that reduction of Cu(II) triggers a catalytic process (Figure 3). To confirm that direct electrode reduction of EBiB was not contributing to the observed peak enhancement, cyclic voltammetry of the initiator was investigated in the absence of the copper complex. EBiB is reduced irreversibly at potentials more than 1.0 V more negative than E° of $[Br Cu^{II}TPMA]^{+}$ (Figure S3 and Table S3).

The mechanism of the process underlying the catalytic peak is illustrated in Scheme 3. Electroreduction of $[Br Cu^{II}TPMA]^{+}$ yields $[Br Cu^{I}TPMA]$, which reversibly dissociates to Br^{-} and $[Cu^{I}TPMA]^{+}$. The latter then reacts with the initiator RBr to give $[Br Cu^{II}TPMA]^{+}$ and $R^{\bullet}$, which terminates via radical coupling mainly with the nitroxyl radical TEMPO. Information on the kinetics of the activation reaction can be obtained by analysis of the catalytic current as a function of scan rate and the ratio

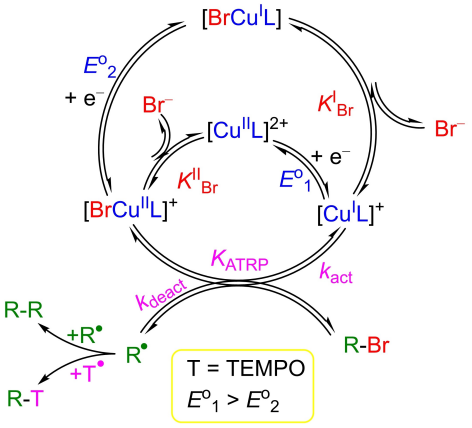

Scheme 3. Mechanism of $[BrCu^{II}L]^+$ reduction in the presence of initiator RBr and radical scavenger TEMPO (T).

between initiator and catalyst concentrations, $\gamma = C_{RBr}/C_{cat}$. This method, known as homogeneous redox catalysis (HRC),[25,33,50–53] is based on fitting of experimental data on working curves appropriately designed according to the mechanism of the electrocatalytic process. A parameter known as degree of catalysis (i_p/i_p^0) is calculated as the ratio between the catalytic peak current, i_p, and the peak current of the catalyst, i_p^0, measured before addition of the initiator. i_p/i_p^0 depends on γ and a kinetic parameter defined as $\lambda = RTk_{act}C_{cat}/Fv$, where k_{act} is the rate constant of the electron transfer between the reduced catalyst and RBr in solution. The working curves can be constructed by digital simulation of cyclic voltammetry (CV) under catalytic conditions, provided that data on various parameters pertinent to the process are available. The aim of the working curve is to define a relationship between i_p/i_p^0 and the kinetic parameter, λ. Therefore, the starting point of CV simulation is to define λ by inserting in the program C_{cat}, and variable values of k_{act} and v. Note that different combinations of these parameters can be used to define a single value of λ, which will correspond to a single value of i_p/i_p^0. Since in the process of working curves construction values of k_{act} are fed to the program to define λ, simulation requires either K_{ATRP} or k_{deact} as $K_{ATRP} = k_{act}/k_{deact}$. We chose to fix K_{ATRP} in the simulation program so that no a priori knowledge of k_{deact} was required.

According to Scheme 3, digital simulation of CVs requires knowledge of redox properties of $[BrCu^{II}TPMA]^+$ and $[Cu^{II}TPMA]^{2+}$, the equilibrium and rate constants of binding of Br^- to $[Cu^{II}TPMA]^{2+}$ and $[Cu^{I}TPMA]^+$, the equilibrium constant of the activation step, K_{ATRP}, and the rate constants of radical coupling reactions. Most of these data are available in the literature. The rate constants of radical trapping with TEMPO as well as radical-radical coupling rate constants have been previously reported.[47–49] Values of E° and k° have been recently reported for both $[Cu^{II}TPMA]^{2+}$ and $[BrCu^{II}TPMA]^+$ in MeCN, DMF and DMSO and their mixtures with styrene,[45] while values for all other systems were measured here as previously described (see for example Figure 1). The diffusion coefficients of $[Cu^{II}TPMA]^{2+}$, $[BrCu^{II}TPMA]^+$ and ethyl α-bromoisobutyrate were measured by cyclic voltammetry (see supporting information).

Regarding the association of Br^- with $[Cu^{II}TPMA]^{2+}$ and $[Cu^{I}TPMA]^+$, recent reports have provided the equilibrium constants, K^{II}_{Br} and K^{I}_{Br} respectively, as well as the rate constants in MeCN, DMF and DMSO.[36] However, there is currently no data available for mixtures of these solvents with methyl methacrylate (MMA) and styrene (STY). To address this gap, spectrophotometric titrations of $[Cu^{II}TPMA]^{2+}$ with Et_4NBr, conducted in the presence of 0.1 M Et_4NBF_4 to maintain a constant ionic strength, were used to determine K^{II}_{Br} in these solvent mixtures. Figure 4a provides an example of titration, displaying the Vis-NIR spectra of $[Cu^{II}TPMA]^{2+}$ in MeCN/STY upon different additions of Br^-. To extract K^{II}_{Br} from the spectra, we utilized the HypSpec software, which is part of the Hyperquad package,[54] at various wavelengths in the range from 600 nm to 1250 nm. Examples of fitting curves are shown in Figure 4b and Figure S4. The measured K^{II}_{Br} values are collected in Table 2.

The binding constants of Br^- to $[Cu^{I}TPMA]^+$ were calculated by equation 4, which combines the standard reduction potentials of the Cu(II) complexes and the Br^- association constants in a thermochemical square scheme (Scheme S1). The obtained K^{I}_{Br} values are reported in Table 2.

$$K^{I}_{Br} = K^{II}_{Br}\exp\left[\frac{F}{RT}\left(E^\circ_{[BrCu^{II}L]^+/[BrCu^{I}L]} - E^\circ_{[Cu^{II}L]^{2+}/[Cu^{I}L]^+}\right)\right] \quad (4)$$

Regarding the association rate constants of Br^- to $[Cu^{II}L]^{2+}$ and $[Cu^{I}L]^+$, $k^{II}_{ass,\ Br^-}$ and $k^{I}_{ass,\ Br^-}$ respectively, we used the values

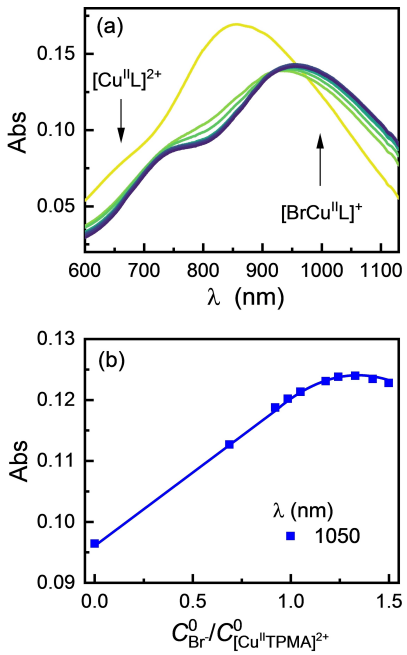

Figure 4. (a) Vis-NIR spectra of $[Cu^{II}TPMA]^{2+}$ solutions ($C^0 = 0.35$ mM, $V^0 = 5$ mL) at 25 °C in MeCN/STY (1:1, v/v) + 0.1 M Et_4NBF_4 after progressive additions of small aliquots of 7.5 mM Et_4NBr in the same medium. (b) Values of absorbance measured during titration at 1050 nm (dots) and the best-fit curve (line).

Table 2. Association constants of Br^- with $[Cu^{II}TPMA]^{2+}$ and $[Cu^{I}TPMA]^{+}$ at 25 °C.

Solvent	Monomer[a]	E_1^o [b] [V]	E_2^o[b] [V]	K_{Br}^{II} [c] [M^{-1}]	K_{Br}^{I} [d] [M^{-1}]
MeCN	–	−0.408[e]	−0.658[e]	3.4×10^{7}[f]	2.02×10^{3}
DMF	–	−0.621[e]	−0.708[e]	4.2×10^{5}[f]	1.42×10^{4}
DMSO	–	−0.615[e]	−0.687[e]	1.0×10^{5}[f]	6.07×10^{3}
MeCN	MMA	−0.410	−0.701	3.9×10^{6}	4.8×10^{1}
DMF	MMA	−0.576	−0.724	3.45×10^{5}	1.09×10^{3}
DMSO	MMA	−0.584	−0.719	1.02×10^{5}	5.33×10^{2}
MeCN	STY	−0.384[e]	−0.683[e]	1.7×10^{6}	1.6×10^{1}
DMF	STY	−0.505[e]	−0.710[e]	7.76×10^{5}	2.66×10^{2}
DMSO	STY	−0.514[e]	−0.693[e]	1.1×10^{7}	1.0×10^{4}

[a] MMA = methyl methacrylate; STY = styrene, both at 50 vol%. [b] vs Fc^+/Fc. [c] Binding constant of Br^- to $[Cu^{II}TPMA]^{2+}$. [d] Binding constant of Br^- to $[Cu^{I}TPMA]^{+}$ calculated by eq. 4. [e] Taken from Ref. [45]. [f] Taken from Ref. [36].

previously reported for the pure solvents, while the simulation program automatically calculated the corresponding $[BrCu^{II}L]^+$ and $[BrCu^{I}L]$ dissociation rate constants from the equilibrium binding constant and association rate constants. The last parameter required by the simulation program is the equilibrium constant, K_{ATRP}, of the initiation step. Values of K_{ATRP} for the reaction of $[Cu^{I}TPMA]^+$ with EBiB were reported only in DMF (1.8×10^{-3})[36] and MeCN (9.6×10^{-6}).[24] However, the degree of catalysis is strongly affected only if $K_{ATRP} < 10^{-5}$; it becomes independent of ATRP equilibrium constant at K_{ATRP} values $\geq 10^{-4}$ (Figure S5). Therefore, for each system we constructed a series of working curves at different K_{ATRP} values, using at least two C_{RBr}/C_{cat} values. Fitting of the experimental data to the working curves allowed not only determination of k_{act} but also estimation of K_{ATRP}. It must be stressed that for some systems K_{ATRP} could not be estimated as the best fit was obtained with $K_{ATRP} \geq 10^{-4}$, where all working curves overlapped each other (e.g. Figure 5). An example of k_{act} determination by this approach is shown in Figure 5 for the activation reaction in DMSO, whereas fitting of data to theoretical curves for all other systems are reported in Figures S6–S8. The values of k_{act} determined by this method are included in Table 1, whereas estimated values of K_{ATRP} are reported in Table S4.

For the sake of comparison, some k_{act} values were measured using both the RDE method and the homogeneous redox catalysis approach, obtaining similar k_{act} values (Table 1, entry 8 vs 9, 10 vs 11, and 13 vs 14).

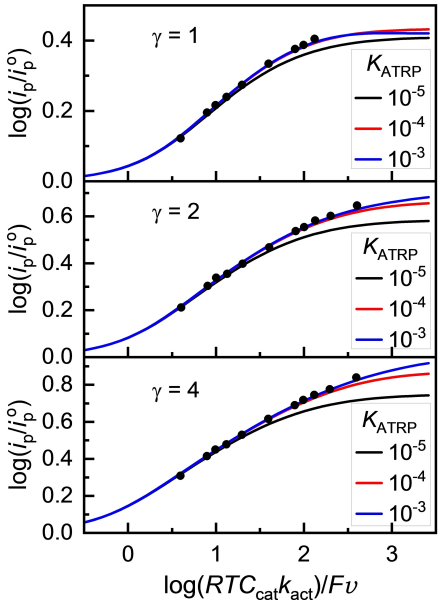

Figure 5. Determination of k_{act} for the reduction of EBiB by $[Cu^{I}TPMA]^+$ in DMSO at 25 °C by fitting of the experimental data (circles) on theoretical working curves (lines). The reaction mixture contains 10^{-3} M $[Cu^{II}TPMA]^{2+}$, 2×10^{-3} M Et_4NBr, 1.93×10^{-2} M TEMPO and EBiB at different concentrations indicated by the excess factor $\gamma = C_{RBr}/C_{cat}$ values reported in the figure. The theoretical curves were calculated for different values of K_{ATRP} as indicated in the figure.

Solvent and Monomer Effects on k_{act}

The set of k_{act} values in pure solvents (Table 1) shows a general trend that activation becomes faster as the polarity of the solvent increases. Solvent effects on kinetic data are often analyzed by the linear solvation energy relationship developed by Taft and Kamlet:[55–59]

$$logk = logk_0 + s(\pi^* + d\delta) + a\alpha + b\beta + h(\delta_H)^2 \quad (5)$$

where π^* stands for the solvent polarity/polarizability, α and β represent the ability of the solvent to donate or accept a proton in a hydrogen bond solute-solvent interaction, respectively, and δ_H is the Hildebrand solubility parameter. The parameter δ in eq. 5 is a polarizability correction term for polychlorinated and aromatic solvents for which δ = 0.5 and 1, respectively. Horn and Matyjaszewski[39] previously analyzed activation rate constants for EBiB by $Cu^{I}Br$/HMTETA (HMTETA = 1,1,4,7,10,10-hexamethyltriethylenetetramine) in a large set of organic solvents. They found that a multiparameter linear fitting of $\log k_{act}$ data to eq. 5 gave a fairly good correlation dominated by the polarity/polarizability parameter. A slightly better correla-

tion was obtained by using only π* after excluding from the analysis a series of alcohols for which the ability of acting as hydrogen bond donors could not be neglected. A linear free energy relationship approach applied to a rather broad range of k_{act} values further showed that π* is a good descriptor of the solvent effect on the ATRP activation step.[42]

In our case, the limited number of solvents (only 5) does not allow meaningful multiparameter regression with eq. 5 as the number of adjustable parameters is bigger than the number of k_{act} values. However, as shown in Figure 6a, logk_{act} showed a good linear correlation with π* ($R^2 = 0.946$). The value of logk_{act} for anisole is out of line because being an aromatic solvent its polarity/polarizability parameter (π* = 0.73) needs the additional correction term $d\delta$ in eq. 5. To determine the correction term, a 2-parameter linear regression considering only π* and the polarizability correction term δ (eq. 6) was used. This gave logk_{act} = −0.144 + 5.615(π*−0.095δ) with $R^2 = 0.999$.

$$logk = logk_0 + s(\pi^* + d\delta) \quad (6)$$

The corrected value of π* for anisole (δ = 1) was thus calculated as 0.64. Correlation of logk_{act} with π* now gave a straight line (Figure 6b), which could be used to predict k_{act} values for other solvents provided that their π* values are known, and they are not good hydrogen bond acceptors or donors such as alcohols.

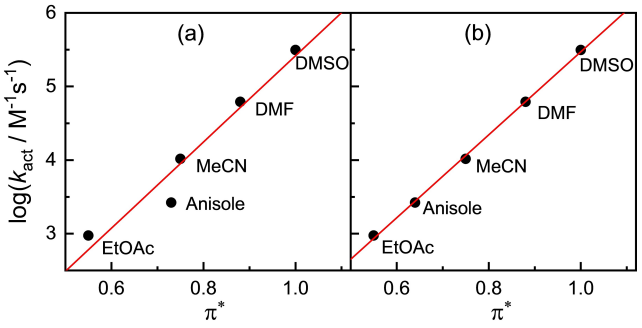

Figure 6. Correlations of k_{act} with the solvent dipolarity/polarizability parameter (a) before and (b) after correction of anisole π*.

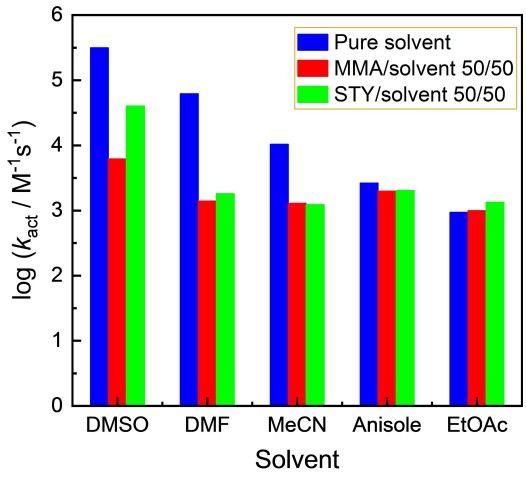

Figure 7. Comparison of k_{act} values obtained in different solvents and solvent/monomer mixtures at 25 °C.

A comparison between activation rate constants in pure solvents and solvent/monomer mixtures (50/50, v/v) is shown in Figure 7. Addition of either styrene or MMA to DMSO, DMF or MeCN decreases k_{act} by about 1–2 orders of magnitude, with the highest k_{act} drop for the most polar solvents, i.e., DMSO and DMF. In contrast, there is no appreciable monomer effect for the two nonpolar solvents. k_{act} slightly decreases in anisole, whereas it slightly increases in nonpolar ethyl acetate when either MMA or STY is added. Since both monomers are considerably less polar than DMSO, DMF and MeCN (relative permittivity ε_r: 37−47 for the solvents and 6.32 and 2.47 for MMA and STY, respectively),[60] their presence in these solvents decreases the polarity/polarizability of the medium resulting in lowering of k_{act}. Although the principal effect of monomers on k_{act} is most likely associated with medium polarity lowering, some contribution due to monomer coordination to Cu(I) cannot be excluded.[43,61,62] On the other hand, anisole and EtOAc have low polarity similar to that of the monomers (ε_r = 6.08 and 4.30 for EtOAc and anisole, respectively),[60] so that mixing MMA or STY with these solvents does not affect the polarity/polarizability parameter of the medium. Interestingly, the presence of monomers in the reaction medium can attenuate the solvent effect on k_{act} by reducing its value. This results in the activation reaction occurring at similar rates across different solvent/monomer mixtures, with the one exception of the highly polar DMSO/monomer mixture.

A last observation is on K_{ATRP} and k_{deact} (Table S4). Unfortunately, the HRC method allowed determination of K_{ATRP}, and hence k_{deact}, only for few of the investigated systems, namely MeCN, and mixtures of MeCN and DMF with STY and MMA. For all of these systems the medium effect on K_{ATRP} roughly matches that on k_{act}. Therefore, k_{deact} is not much affected.

Conclusions

The kinetics of ethyl α-bromoisobutyrate activation by $[Cu^{I}TPMA]^+$ shows a strong solvent dependence with k_{act} values decreasing from 3.14×10^5 mol^{-1} dm^3 s^{-1} in DMSO down to 9.41×10^2 mol^{-1} dm^3 s^{-1} in ethyl acetate. Addition of styrene or methyl methacrylate (50 vol%) to highly polar solvents such as DMSO, DMF and MeCN considerably lowers the activation rate constants. Conversely, k_{act} is little affected by the presence of monomers in nonpolar solvents such as anisole and ethyl acetate. These observations were rationalized by correlating the rate constants with the medium polarity. Indeed, logk_{act} in pure solvents shows an excellent linear correlation with the solvent polarity/polarizability parameter π*. In pure solvents, greater polarity leads to faster activation reactions, and this trend is expected to apply to solvent/monomer mixtures as well. The effect of MMA and STY on k_{act} is therefore linked to the extent to which these monomers alter the polarity of the polymerization medium (monomer + solvent). For highly polar solvents, the medium π* decreases in the presence of a monomer, leading to a drop of k_{act} values, whereas in less polar solvents,

there is no significant change of π^*, and consequently k_{act} remains relatively unchanged. This last observation is particularly important as it shows that the common assumption that the addition of monomers decreases k_{act} in all solvents is not always true.

Experimental Section

Chemicals

Dimethyl sulfoxide (DMSO, Sigma-Aldrich, anhydrous, 99.9%), acetonitrile (MeCN, Sigma-Aldrich, anhydrous, 99.8%), anisole (Sigma-Aldrich, anhydrous 99.7), ethyl acetate (EtOAc, Sigma-Aldrich, anhydrous 99.8%), *N*,*N*-dimethylformamide (DMF, Sigma-Aldrich, anhydrous, 99.8%), tris(2-pyridylmethyl)amine (TPMA, Tokyo Chemical Industries, $\geq$ 98%), 2,2,6,6-tetramethyl-1-piperidinyloxy (TEMPO, Sigma-Aldrich, 98%), ethyl α-bromoisobutyrate (EBiB, Sigma-Aldrich, 98%), and Copper(II) trifluoromethanesulfonate ($Cu(CF_3SO_3)_2$, Alfa Aesar, 98%) were used as received. Methyl methacrylate (MMA, Sigma-Aldrich, 99%) and styrene (STY, Sigma-Aldrich, 99%) were percolated through a column filled with basic Al_2O_3 to remove the polymerization inhibitors.

Tetraethylammonium tetrafluoroborate (Et_4NBF_4, Alfa Aesar, 99%), the supporting electrolyte used for most experiments, was recrystallized twice from ethanol and dried in a vacuum oven at 70 °C for 48 h. In low polarity media, such as anisole, EtOAc, and their mixtures with MMA and STY, tetrabutylammonium tetrafluoroborate (*n*-Bu_4NBF_4, Sigma-Aldrich, 99%) was used as the supporting electrolyte; it was recrystallized from double-distilled water and dried in a vacuum oven at 80 °C for 48 h. Tetraethylammonium bromide (Et_4NBr, Sigma-Aldrich, 99%), used as a source of Br^- ions in complexation titrations, was recrystallized from acetone and dried at 70 °C under vacuum for 48 h.

A stock solution of $Cu^I(CF_3SO_3)$ in MeCN was prepared starting from copper(II) triflate. A weighed amount of the salt was dissolved in MeCN in a deoxygenated vial containing an activated copper wire (activated by dipping in HCl/MeOH 1/3, rinsing in MeOH, and then drying under nitrogen). After further deoxygenation by bubbling Ar through the solution for 15 min, the vial was closed and left for 24 h for the production of Cu(I) by comproportionation of Cu(II) with Cu(0). The stock Cu(I) solution was standardized by spectrophotometric analysis using 2,9-dimethyl-1,10-phenantroline as a specific ligand ($\varepsilon = 8000\ M^{-1}cm^{-1}$ at 455 nm in MeCN[63]), in a 3-fold excess over Cu(I)[64].

Instrumentation

An Autolab PGSTAT 30 potentiostat/galvanostat, equipped with GPES software (Metrohm AG, The Netherlands) was used for all electrochemical experiments. A three-electrode cell with a 3 mm glassy carbon (GC) disk working electrode (Tokai GC-20), a Pt wire counter electrode and Ag|AgI|*n*-Bu_4NI (0.1 M in DMF) reference electrode was used. The cell was thermostated at 25 °C, and all experiments were performed under argon atmosphere. The Ag|AgI|*n*-Bu_4NI reference electrode was always calibrated with the ferrocenium/ferrocene couple (Fc^+/Fc) used as an internal standard, and the potentials were converted to the Fc^+/Fc scale to which all potentials are reported. Before each experiment, the GC disk was cleaned by polishing with a 0.25-μm diamond paste, followed by ultrasonic rinsing in ethanol for 5 min. Activation rate constants were determined by cyclic voltammetry or chronoamperometry. In the latter case, the working electrode was a rotating disc electrode with a 3-mm GC tip (Metrohm AG, The Netherlands).

Spectrophotometric titrations of $[Cu^{II}TPMA]^{2+}$ solutions with bromide ions were carried out with an Agilent Cary 5000 spectrophotometer by using 10 mm or 40 mm optical path length quartz cuvettes. The HypSpec 2014 software from Hyperquad was used to elaborate the spectrophotometric data for binding constant determination.

Working curves for the determination of rate constants were constructed by digital simulation of cyclic voltammetry of catalytic systems; simulations were performed with DigiSim 3.03 (Bioanalytical Systems, Inc.).

All experiments were performed in a jacketed cell with a fixed temperature of 25 °C.

Supporting Information

The authors have cited additional references within the Supporting Information.[65]

Acknowledgements

This work is funded by the European Union – NextGenerationEU and by the 2021 STARS Grants@Unipd programme (photo-e-cat).

Conflict of Interests

The authors declare no conflict of interest.

Data Availability Statement

The data that support the findings of this study are available in the supplementary material of this article.

Keywords: Activation kinetics · ATRP · medium effect · copper catalyst · LSER

[1] K. Matyjaszewski, N. V. Tsarevsky, *J. Am. Chem. Soc.* **2014**, *136*, 6513–6533.
[2] F. Lorandi, M. Fantin, K. Matyjaszewski, *J. Am. Chem. Soc.* **2022**, *144*, 15413–15430.
[3] C. Y. Lin, M. L. Coote, A. Gennaro, K. Matyjaszewski, *J. Am. Chem. Soc.* **2008**, *130*, 12762–12774.
[4] A. A. Isse, A. Gennaro, C. Y. Lin, J. L. Hodgson, M. L. Coote, T. Guliashvili, *J. Am. Chem. Soc.* **2011**, *133*, 6254–6264.
[5] A. A. Isse, N. Bortolamei, P. De Paoli, A. Gennaro, *Electrochim. Acta* **2013**, *110*, 655–662.
[6] C. Fang, M. Fantin, X. Pan, K. de Fiebre, M. L. Coote, K. Matyjaszewski, P. Liu, *J. Am. Chem. Soc.* **2019**, *141*, 7486–7497.
[7] J.-S. Wang, K. Matyjaszewski, *J. Am. Chem. Soc.* **1995**, *117*, 5614–5615.
[8] M. Kato, M. Kamigaito, M. Sawamoto, T. Higashimura, *Macromolecules* **1995**, *28*, 1721–1723.
[9] X. Pan, M. Fantin, F. Yuan, K. Matyjaszewski, *Chem. Soc. Rev.* **2018**, *47*, 5457–5490.
[10] W. A. Braunecker, K. Matyjaszewski, *Prog. Polym. Sci.* **2007**, *32*, 93–146.

[11] T. G. Ribelli, F. Lorandi, M. Fantin, K. Matyjaszewski, *Macromol. Rapid Commun.* **2019**, *40*, 1800616.
[12] J. Wang, J. Han, X. Xie, Z. Xue, C. Fliedel, R. Poli, *Macromolecules* **2019**, *52*, 5366–5376.
[13] G. Gazzola, S. Pasinato, M. Fantin, N. Braidi, C. Tubaro, C. Durante, A. A. Isse, *Molecules* **2022**, *27*, 6312.
[14] S. Dadashi-Silab, K. Kim, F. Lorandi, D. J. Schild, M. Fantin, K. Matyjaszewski, *Polym. Chem.* **2022**, *13*, 1059–1066.
[15] X. Pan, N. Malhotra, J. Zhang, K. Matyjaszewski, *Macromolecules* **2015**, *48*, 6948–6954.
[16] X. Pan, N. Malhotra, S. Dadashi-Silab, K. Matyjaszewski, *Macromol. Rapid Commun.* **2017**, *38*, 1600651.
[17] G. Gazzola, A. Antonello, A. A. Isse, M. Fantin, *ACS Macro Lett.* **2023**, *12*, 1602–1607.
[18] X. Pan, N. Malhotra, A. Simakova, Z. Wang, D. Konkolewicz, K. Matyjaszewski, *J. Am. Chem. Soc.* **2015**, *137*, 15430–15433.
[19] W. Zhang, J. He, C. Lv, Q. Wang, X. Pang, K. Matyjaszewski, X. Pan, *Macromolecules* **2020**, *53*, 4678–4684.
[20] J. He, W. Zhang, C. Lv, R. Chen, L. Wang, Y. Wang, X. Pan, *Polymer (Guildf)* **2021**, *215*, 123345.
[21] X. Pan, C. Fang, M. Fantin, N. Malhotra, W. Y. So, L. A. Peteanu, A. A. Isse, A. Gennaro, P. Liu, K. Matyjaszewski, *J. Am. Chem. Soc.* **2016**, *138*, 2411–2425.
[22] G. Yilmaz, Y. Yagci, *Polym. Chem.* **2018**, *9*, 1757–1762.
[23] D. A. Corbin, G. M. Miyake, *Chem. Rev.* **2022**, *122*, 1830–1874.
[24] W. Tang, Y. Kwak, W. Braunecker, N. V. Tsarevsky, M. L. Coote, K. Matyjaszewski, *J. Am. Chem. Soc.* **2008**, *130*, 10702–10713.
[25] M. Fantin, A. A. Isse, K. Matyjaszewski, A. Gennaro, *Macromolecules* **2017**, *50*, 2696–2705.
[26] M. Fantin, A. A. Isse, A. Gennaro, K. Matyjaszewski, *Macromolecules* **2015**, *48*, 6862–6875.
[27] T. Pintauer, W. Braunecker, E. Collange, R. Poli, K. Matyjaszewski, *Macromolecules* **2004**, *37*, 2679–2682.
[28] W. Tang, K. Matyjaszewski, *Macromolecules* **2007**, *40*, 1858–1863.
[29] F. Seeliger, K. Matyjaszewski, *Macromolecules* **2009**, *42*, 6050–6055.
[30] C. A. Bell, P. V. Bernhardt, M. J. Monteiro, *J. Am. Chem. Soc.* **2011**, *133*, 11944–11947.
[31] M. Fantin, A. A. Isse, N. Bortolamei, K. Matyjaszewski, A. Gennaro, *Electrochim. Acta* **2016**, *222*, 393–401.
[32] T. G. Ribelli, M. Fantin, J.-C. Daran, K. F. Augustine, R. Poli, K. Matyjaszewski, *J. Am. Chem. Soc.* **2018**, *140*, 1525–1534.
[33] D. Konkolewicz, P. Krys, J. R. Góis, P. V. Mendonça, M. Zhong, Y. Wang, A. Gennaro, A. A. Isse, M. Fantin, K. Matyjaszewski, *Macromolecules* **2014**, *47*, 560–570.
[34] S. Smolne, M. Buback, *Macromol. Chem. Phys.* **2015**, *216*, 894–902.
[35] P. Pavan, F. Lorandi, F. De Bon, A. Gennaro, A. A. Isse, *ChemElectroChem* **2021**, *8*, 2450–2458.
[36] M. Fantin, F. Lorandi, T. G. Ribelli, G. Szczepaniak, A. E. Enciso, C. Fliedel, L. Thevenin, A. A. Isse, R. Poli, K. Matyjaszewski, *Macromolecules* **2019**, *52*, 4079–4090.
[37] A. E. Enciso, F. Lorandi, A. Mehmood, M. Fantin, G. Szczepaniak, B. G. Janesko, K. Matyjaszewski, *Angew. Chem. Int. Ed.* **2020**, *59*, 14910–14920.
[38] F. Lorandi, M. Fantin, A. A. Isse, A. Gennaro, *Polymer (Guildf)* **2015**, *72*, 238–245.
[39] M. Horn, K. Matyjaszewski, *Macromolecules* **2013**, *46*, 3350–3357.
[40] N. Bortolamei, A. A. Isse, V. B. Di Marco, A. Gennaro, K. Matyjaszewski, *Macromolecules* **2010**, *43*, 9257–9267.
[41] P. De Paoli, A. A. Isse, N. Bortolamei, A. Gennaro, *Chem. Commun.* **2011**, *47*, 3580.
[42] F. Lorandi, M. Fantin, H. Jafari, A. Gorczynski, G. Szczepaniak, S. Dadashi-Silab, A. A. Isse, K. Matyjaszewski, *J. Am. Chem. Soc.* **2023**, *145*, 21587–21599.
[43] T. Pintauer, K. Matyjaszewski, *Coord. Chem. Rev.* **2005**, *249*, 1155–1184.
[44] S. Racioppi, L. Orian, C. Tubaro, A. Gennaro, A. A. Isse, *Catalysts* **2022**, *12*, 1656.
[45] F. De Bon, G. M. Carlan, E. Tognella, A. A. Isse, *Processes* **2021**, *9*, 1327.
[46] R. S. Nicholson, *Anal. Chem.* **1965**, *37*, 1351–1355.
[47] A. L. J. Beckwith, V. W. Bowry, K. U. Ingold, *J. Am. Chem. Soc.* **1992**, *114*, 4983–4992.
[48] N. V. Lebedeva, D. P. Zubenko, E. G. Bagryanskaya, R. Z. Sagdeev, G. S. Ananchenko, S. Marque, D. Bertin, P. Tordo, *Phys. Chem. Chem. Phys.* **2004**, *6*, 2254–2259.
[49] H. Paul, H. Fischer, *Acc. Chem. Res.* **1987**, *20*, 200–206.
[50] C. P. Andrieux, J. M. Dumas-Bouchiat, J. M. Saveant, *J. Electroanal. Chem. Interfacial Electrochem.* **1978**, *87*, 55–65.
[51] C. P. Andrieux, C. Blocman, J. M. Dumas-Bouchiat, F. M'Halla, J. M. Savéant, *J. Electroanal. Chem. Interfacial Electrochem.* **1980**, *113*, 19–40.
[52] C. P. Andrieux, C. Blocman, J. M. Dumas-Bouchiat, J. M. Saveant, *J. Am. Chem. Soc.* **1979**, *101*, 3431–3441.
[53] A. A. Isse, A. Gennaro, *J. Phys. Chem. A* **2004**, *108*, 4180–4186.
[54] P. Gans, A. Sabatini, A. Vacca, *Talanta* **1996**, *43*, 1739–1753.
[55] M. J. Kamlet, J.-L. M. Abboud, M. H. Abraham, R. W. Taft, *Solvent Effects in Organic Chemistry*, Verlag, **1983**.
[56] M. H. Abraham, R. M. Doherty, M. J. Kamlet, J. M. Harris, R. W. Taft, *J. Chem. Soc. Perkin Trans. 2* **1987**, *11*, 1097.
[57] R. M. C. Gonçalves, L. M. P. C. Albuquerque, *J. Phys. Org. Chem.* **2001**, *14*, 731–736.
[58] R. Castro-Olivares, G. Günther, A. L. Zanocco, E. Lemp, *J. Photochem. Photobiol. A* **2009**, *207*, 160–166.
[59] J. B. Nikolić, G. S. Uščumlić, I. O. Juranić, *Int. J. Chem. Kinet.* **2010**, *42*, 430–439.
[60] C. Wohlfarth, in *CRC Handbook of Chemistry and Phyiscs* (Ed.: D. R. Lide), Taylor And Francis, Boca Raton, FL, **2007**.
[61] W. A. Braunecker, N. V. Tsarevsky, T. Pintauer, R. R. Gil, K. Matyjaszewski, *Macromolecules* **2005**, *38*, 4081–4088.
[62] W. A. Braunecker, T. Pintauer, N. V. Tsarevsky, G. Kickelbick, Krzysztof Matyjaszewski, *J. Organomet. Chem.* **2005**, *690*, 916–924.
[63] M. Meyer, A. M. Albrecht-Gary, C. O. Dietrich-Buchecker, J. P. Sauvage, *Inorg. Chem.* **1999**, *38*, 2279–2287.
[64] A. R. Gahler, *Anal. Chem.* **1954**, *26*, 577–579.
[65] A. A. Isse, G. Berzi, L. Falciola, M. Rossi, P. R. Mussini, A. Gennaro, *J. Appl. Electrochem.* **2009**, *39*, 2217–2225.

Manuscript received: November 12, 2023
Revised manuscript received: January 19, 2024
Version of record online: ■■, ■■

RESEARCH ARTICLE

Unlike classical radical polymerization, the kinetics of atom transfer radical polymerization (ATRP) are highly influenced by the solvent. We conducted an electrochemical study on ATRP activation kinetics (k_{act}) in 15 solvent/monomer combinations, revealing a strong correlation with solvent polarity/polarizability. The addition of a monomer to a polar solvent significantly diminished k_{act}, while in nonpolar solvents it barely affected k_{act}.

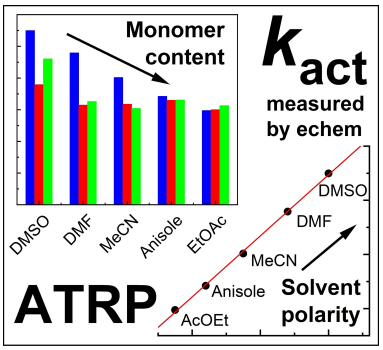

*Dr. M. Fantin, E. Tognella, A. Antonello, Dr. F. Lorandi, E. Calore, A. Macior, Prof. C. Durante, Prof. A. A. Isse**

1 – 10

Effects of Solvent and Monomer on the Kinetics of Radical Generation in Atom Transfer Radical Polymerization